Inorg. Chem. **2003**, *42*, 1982–1993

Inorganic Chemistry

Article

Structure and Bonding in Solution of Dioxouranium(VI) Oxalate Complexes: Isomers and Intramolecular Ligand Exchange

Valérie Vallet,*,[†],[‡],[§] Henry Moll,[||] Ulf Wahlgren,[†] Zoltán Szabó,[⊥] and Ingmar Grenthe*,[⊥]

Institute of Physics, Stockholm University, P.O. Box 6730, S-11385 Stockholm, Sweden, Institute of Quantum Physics, Paul Sabatier University, F-31062 Toulouse, France, Institute of Physical and Theoretical Chemistry, Technical University of Munich, D-85747 Garching, Germany, Institut für Radiochemie, Forschungszentrum Rossendorf, e.V., D-01314 Dresden, Germany, and Inorganic Chemistry, Department of Chemistry, Royal Institute of Technology (KTH), S-10044 Stockholm, Sweden

Received September 28, 2002

Structural isomers of $[UO_2(\text{oxalate})_3]^{4-}$, $[UO_2(\text{oxalate})F_3]^{3-}$, $[UO_2(\text{oxalate})_2F]^{3-}$, and $[UO_2(\text{oxalate})_2(H_2O)]^{2-}$ have been studied by using EXAFS and quantum chemical ab initio methods. Theoretical structures and their relative energies were determined in the gas phase and in water using the CPCM model. The most stable isomers according to the quantum chemical calculations have geometries consistent with the EXAFS data, and the difference between measured and calculated bond distances is generally less than 0.05 Å. The complex $[UO_2(\text{oxalate})_3]^{4-}$ contains two oxalate ligands forming five-membered chelate rings, while the third is bonded end-on to a single carboxylate oxygen. The most stable isomer of the other two complexes also contains the same type of chelate-bonded oxalate ligands. The activation energy for ring opening in $[UO_2(\text{oxalate})F_3]^{3-}$, $\Delta U^{\ddagger} = 63$ kJ/mol, is in fair agreement with the experimental activation enthalpy, $\Delta H^{\ddagger} = 45 \pm 5$ kJ/mol, for different $[UO_2(\text{picolinate})F_3]^{2-}$ complexes, indicating similar ring-opening mechanisms. No direct experimental information is available on intramolecular exchange in $[UO_3(\text{oxalate})_3]^{4-}$. The theoretical results indicate that it takes place via the tris-chelated intermediate with an activation energy of $\Delta U^{\ddagger} = 38$ kJ/mol; the other pathways involve multiple steps and have much higher activation energies. The geometries and energies of dioxouranium(VI) complexes in the gas phase and solvent models differ slightly, with differences in bond distance and energy of typically less than 0.06 Å and 10 kJ/mol, respectively. However, there might be a significant difference in the distance between uranium and the leaving/entering group in the transition state, resulting in a systematic error when the gas-phase geometry is used to estimate the activation energy in solution. This systematic error is about 10 kJ/mol and tends to cancel when comparing different pathways.

Introduction

The structures of solid uranium(VI) oxalate compounds reveal different modes of bonding of the ligand chelated through one oxygen from each carboxylate group,[1−3] coordinated through two oxygen atoms of the same carboxylate group,[4,5] or bonded to a single carboxylate oxygen.[6,7] In most of these structures, the oxalate is bridging different uranyl units. The composition of the complexes have previously been determined by equilibrium analytical methods,[8−10] but

---

* Authors to whom correspondence should be addressed. E-mail: valerie.vallet@ch.tum.de (V.V.), ingmarg@kth.se (I.G.). Fax: +49-89-289-13622 (V.V.), +46-8-212626 (I.G.).

[†] Stockholm University.

[‡] Paul Sabatier University.

[§] Technical University of Munich.

[||] Forschungszentrum Rossendorf, e.V.

[⊥] Royal Institute of Technology (KTH).

(1) Jayadevan, N. C.; Singh Muder, K. D.; Chackraburtty, D. M. *Acta Crystallogr. B* **1975**, *31*, 2277.

(2) Szabó, Z.; Fischer, A. *Acta Crystallogr. E* **2002**, *58*, i56.

(3) Jayadevan, N. C.; Chackraburtty, D. M. *Acta Crystallogr. B* **1972**, *28*, 3178.

(4) Alcock, N. W. *J. Chem. Soc., Dalton. Trans.* **1973**, 1610.

(5) Alcock, N. W. *J. Chem. Soc., Dalton. Trans.* **1973**, 1616.

(6) Alcock, N. W. *J. Chem. Soc., Dalton. Trans.* **1973**, 1614.

(7) Legros, J. P.; Jeannin, Y. *Acta Crystallogr. B* **1976**, *32*, 2497.

(8) (a) Havel, J. *Collect. Czech. Chem. Commun.* **1969**, *34*, 2348. (b) Havel, J.; Soto-Guerrero, J. and Lubal, P. *Polyhedron* **2002**, *21*, 1411.

(9) Ferri, D.; Iuliano, M.; Manfredi, C.; Vasca, E.; Curaso, T.; Clemente, M.; Fontanella, C. *J. Chem. Soc., Dalton. Trans.* **2000**, 3460.

(10) Aas, W.; Moukhamet-Galeev, A.; Grenthe, I. *Radiochim. Acta* **1998**, *82*, 77.

10.1021/ic026068s CCC: $25.00

Table 1. Results from the EXAFS Study

sample/U(VI) speciation	model	shell[a]	$N^{b,c}$	$r^{b,c}$(Å)	$\sigma^{2\ b,c}$ (Å^2)	ΔE_0 (eV)
A	A1	U−O$_{ax}$	2f^d	1.78	0.0015	−7.7
$UO_2(ox)_2^{2-}$(aq)		U−O$_{eq}$	5.1 ± 0.7	2.38	0.0063	
		U−C	2.6 ± 1.0	3.25	0.0022	
		U−C−O^e	3f	4.47	0.0028	
	A2	U−O$_{ax}$	2f	1.78	0.0015	−7.7
		U−O$_{eq}$	5.1 ± 0.7	2.38	0.0062	
				2.406(1)^{f,g}		
		U−C	4f	3.25	0.0040	
				3.273		
		U−C−O^e	3f	4.47	0.0027	
B	four-shell fit	U−O$_{ax}$	2f	1.79	0.0015	−7.2
$UO_2(ox)_2F^{3-}$		U−F	1f	2.23	0.0030	
				2.219		
		U−O$_{eq}$	4.0 ± 0.9	2.39	0.0063	
				2.436^{f,g}		
		U−C	4f	3.27	0.0047	
				3.307(2)^{f,g}		
		U−C−O^e	3f	4.49	0.0035	
C	C	U−O$_{ax}$	2f	1.79	0.0011	−6.8
$UO_2(ox)_3^{4-}$		U−O$_{eq}$	5f	2.37	0.0054	
			4			
			1			
				2.427(6)^{f,g}		
				2.386		
		U−C	4	3.26	0.0047	
			4	3.302(2)^{f,g}		
		U−C−O^e	3f	4.40	0.0067	
		U−C−O−C^e	4f	4.53	0.0067	
				(4.50)		

[a] Contributions of individual shells to the total EXAFS oscillation in model C are as follows: U−O$_{ax}$, 61%; U−O$_{eq}$, 19%; U−C, 7.5%; MS path of U−O$_{ax}$, 1.7%; and MS paths (three- and four-legged) of U−C−O, 3.2%. [b] N denotes the number of distances from U to O and C within a given shell, r is the corresponding distance in ångströms, and σ^2 is the Debye−Waller factor. [c] 95% confidence limits for the coordination numbers (N) and bond lengths (r) are as follows: U−O$_{ax}$, 8% and ±0.005 Å; U−O$_{eq}$, 17% and ±0.01 Å; U−C, 40% and ±0.08 Å. [d] f = parameter fixed during the fit. [e] MS pathway. [f] Average values from theoretical calculations of the optimized structures in the solvent. The values in parentheses represent the maximum deviations of individual distances from the average values. [g] Average U−O$_{oxalate}$ distance.

with different conclusions[8,9] as to the stability of the $UO_2(oxalate)_3^{4-}$ complex, where the equilibrium constants proposed by Ferri et al.[9] indicate that all oxalates are chelate-bonded, whereas those of Havel[8a] indicate that the third oxalate is singly bonded. However, equilibrium analysis provides no direct information on the formation of isomers, or information on the mode of bonding of ligands, a fact that hampers a more detailed chemical discussion. Information on solution structures can be obtained from either NMR[11] or EXAFS data; in the latter case, the information is limited to radial distances from the central atom to the surrounding atom shells and the number of such distances. The bond distances can generally be determined with an error of 1% or less, whereas the uncertainty in the number of bonds is at best 10%, but in general much larger (cf. Table 1). Hence, the accuracy of the EXAFS data is often not sufficient to discriminate between structures with different modes of coordination and/or coordination numbers but similar metal-to-ligand distances. In previous studies,[12−14] we have demonstrated how quantum chemical methods can be used both to estimate the relative stabilities of isomers and to obtain more precise structure models than from EXAFS data alone.

The main issue in the present study is to determine whether bonding isomers can occur also in aqueous solution and to study their structures, relative stabilities, and mechanisms of interconversion. The inquiry consists of two parts: in the first, we used quantum chemical methods to determine the relative stabilities and structures of different isomers of $[UO_2(oxalate)_2F]^{3-}$, $[UO_2(oxalate)_2(H_2O)]^{2-}$ $[UO_2(oxalate)F_3]^{3-}$, and $[UO_2(oxalate)_3]^{4-}$ and compare these data with structures obtained from solution using EXAFS and from the solid state by single-crystal X-ray diffraction. In the second part, we investigate possible intramolecular exchange mechanisms in $[UO_2(oxalate)F_3]^{3-}$ and $[UO_2(oxalate)_3]^{4-}$. For the former, we do so by comparing activation enthalpies obtained experimentally[15] with those obtained by the ab initio methods described in previous communications,[14,16] whereas for the latter, no experimental data are available. As discussed herein, the identification and modeling of solvent water participation in these reactions is a difficult problem that makes it impossible to calculate the activation entropy with the same accuracy as the experimental value can be measured.

Computational Details and Experimental Investigation

Computational Details. The quantum chemical approach used here is the same as in our previous studies.[13,14] The geometries of

---

(11) Szabó, Z.; Aas, W.; Grenthe, I. *Inorg. Chem.* **1997**, *36*, 5369.

(12) Wahlgren, U.; Moll, H.; Grenthe, I.; Schimmelpfennig, B.; Maron, L.; Vallet, V.; Gropen, O. *J. Phys. Chem. A* **1999**, *103*, 8257.

(13) Vallet, V.; Wahlgren, U.; Schimmelpfennig, B.; Moll, H.; Szabó, Z.; Grenthe, I. *Inorg. Chem.* **2001**, *14*, 3516.

(14) Vallet, V.; Wahlgren, U.; Schimmelpfennig, B.; Szabó, Z.; Grenthe, I. *J. Am. Chem. Soc.* **2001**, *123*, 11999.

(15) Szabó, Z.; Grenthe, I. *Inorg. Chem.* **1998**, *37*, 6214.

(16) Vallet, V.; Wahlgren, U.; Szabó, Z.; Grenthe, I. *Inorg. Chem.* **2002**, *41*, 5126.

all of the compounds were optimized at the Hartree−Fock level without the imposition of symmetry constraints and with the energy contribution of correlation estimated by single-point MP2 calculations at the structure optimized in the solvent. All calculations were performed using the Gaussian 98 package[17] and a solvent model in which the water is described by a conductor-like polarizable continuum medium (CPCM)[18,19] of permittivity $\epsilon_r = 80$. The solute is embedded in a shape-adapted cavity consisting of interlocking spheres centered on each solute atom or group and with standard UATM (united-atomic topological model) radii.[20] Geometry optimizations in solvent often show poor convergence behavior. Following Cosentino et al.,[21] we removed the linear search procedure in the standard Berny algorithm and omitted the nonelectrostatic contributions from cavity formation, dispersion, and repulsion. These contributions, however, were included in the final single-point MP2 calculations. The energies for the stable structures of reactants, intermediates, and products are for the geometries optimized in solvent.

We explored several pathways for intramolecular exchange in $[UO_2(oxalate)F_3]^{3-}$ and $[UO_2(oxalate)_3]^{4-}$. The transition states were identified as described in a previous study.[14] The activation energy for the ring opening/closure in $[UO_2(oxalate)F_3]^{3-}$ was calculated using the geometries optimized in both the gas phase and the solvent. There are a number of possible intramolecular exchange pathways in $[UO_2(oxalate)_3]^{4-}$, and we used the activation energy for the gas-phase geometry as an estimate of their relative activation energies in the solvent. Full geometry optimization within the solvent for all pathways would have been too time-consuming, given the numerous structures that have to be considered to characterize reaction profile C. Moreover, frequency calculations in the solvent can only be done numerically and sometimes lead to several imaginary frequencies of low values. We therefore re-optimized the transition state only for the lowest energy reaction pathway B. The transition state was identified by its single imaginary mode, the same as the one found in the gas-phase optimized structure.

The quantum chemical models give the energy change at 0 K for a static structure. However, the enthalpy, Gibbs energy, and entropy can be calculated from the partition functions for the vibrational and rotational motions. For technical reasons, we only performed frequency analyses on gas-phase structures (analytic second derivatives for the CPCM model are not included in the present version of the Gaussian package). We therefore assumed the vibrations to be identical in vacuum and in solution, following the argument of Tomasi and Persico.[22] It turned out that the difference in the entropic and thermal contributions between the various isomers was small, indicating that the Gibbs energy change $\Delta G°$ is, within a few kilojoules per mole, the same as the total energy change ΔU, as shown in Tables 2−4. Hence, it seems a reasonable approximation to discuss the relative stabilities of various isomers in terms of ΔU.

The rate constants for the ligand exchange reactions can be calculated from the activation free energies from the equation

$$k(T) = (k_B T/h)\exp(-\Delta G^{\ddagger}/RT) \tag{1}$$

where $\Delta G^{\ddagger}$ is the activation free energy, T is the temperature in Kelvin, R is the gas constant, k_B is the Boltzmann constant, and h is Planck's constant. However, as the accuracy of the theory-calculated $\Delta G^{\ddagger}$ is at best 10−20 kJ/mol, which corresponds to 2−4 orders of magnitudes in the rate constant, it makes little sense to discuss experimental and calculated rate constants. We therefore compare only experimental and theoretical activation enthalpies following the arguments detailed in a previous study.[14] The computed vibration frequencies for the stable isomers are given as Supporting Information.

EXAFS Measurements. EXAFS data were recorded at the Rossendorf Beamline (ROBL) at ESRF in Grenoble, France. Transmission spectra were measured at room temperature using a water-cooled Si(111) double-crystal monochromator of fixed-exit type ($E = 5-35$ keV). Higher harmonics were rejected using two Pt-coated mirrors. More information on the EXAFS measurements can be found in refs 23 and 24. The samples had the following composition: solution A 0.0122 M sodium oxalate, 0.0601 uranyl nitrate, pH = 4.4; solution B 0.1208 M potassium oxalate, 0.070 M sodium fluoride, 0.0601 M uranyl nitrate, pH = 4.2; solution C 1.68 M potassium oxalate, 0.0601 M uranyl nitrate, pH = 6.5. Three EXAFS scans were collected from each sample and then averaged. For energy calibration of the sample spectra, the K-edge spectrum (17 038 eV) from an Y foil was recorded simultaneously. The ionization energy of the U L_{III} electron, E_0, was defined as 17 185 eV. The data were treated using the EXAFSPAK software.[25] Theoretical backscattering phase and amplitude functions used in data analysis were calculated for different structures of the model complex $[UO_2(oxalate)_3]^{4-}$ using the FEFF7 program.[26] The MS path O−U−O (four-legged path) of the linear UO_2^{2+} unit and the MS paths U−C−O (three- and four-legged paths) were included in the model calculations. The EXAFS oscillations were isolated using standard procedures for pre-edge subtraction, spline removal, and data normalization.[27] The amplitude reduction factor, S_0^2, was held constant at 0.9 for all fits. The speciation of the different test solutions was calculated from the analytical total concentrations and the known equilibrium constants. Test solutions A and B contained more than 99% of $[UO_2(oxalate)_2(H_2O)]^{2-}$ and $[UO_2(oxalate)_2F]^{3-}$, respectively, whereas solution C contained more than 95% of the complex $[UO_2(oxalate)_3]^{4-}$ (cf. Figure S4b).

Table 1 shows the U−O bond distances, r, in the various shells and the number of these distances, N, using models with three and

---

(17) Frisch, M. J.; Trucks, G. W.; Schlegel, H. B.; Scuseria, G. E.; Robb, M. A.; Cheeseman, J. R.; Zakrzewski, V. G.; Montgomery, J. A.; Stratmann, R. E.; Burant, J. C.; Dapprich, S.; Millam, J. M.; Daniels, A. D.; Kudin, K. N.; Strain, M. C.; Farkas, O.; Tomasi, J.; Barone, V.; Cossi, M.; Cammi, R.; Mennucci, B.; Pomelli, C.; Adamo, C.; Clifford, S.; Ochterski, J.; Petersson, G. A.; Ayala, P. Y.; Cui, Q.; Morokuma, K.; Malick, D. K.; Rabuck, A. D.; Raghavachari, K.; Foresman, J.; Cioslowski, J. B.; Ortiz, J. V.; Stefanov, B. B.; Liu, G.; Liashenko, A.; Piskorz, P.; Komaromi, I.; Gomperts, R.; Martin, R. L.; Fox, D. J.; Keith, T.; Al-Laham, M. A.; Peng, C. Y.; Nanayakkara, A.; Gonzalez, C.; Challacombe, M.; Gill, P. M. W.; Johnson, B. G.; Chen, W.; Wong, M. W.; Andres, J. L.; Head-Gordon, M.; Replogle, E. S.; Pople, J. A. *Gaussian 98*, revision A.9; Gaussian, Inc.: Pittsburgh, PA 1998.

(18) Barone, V.; Cossi, M. *J. Phys. Chem. A* **1998**, *102*, 1995.

(19) Cossi, M.; Barone, V. *J. Chem. Phys.* **1998**, *109*, 6246.

(20) Barone, V.; Cossi, M.; Tomasi, J. *J. Chem. Phys.* **1997**, *107*, 3210.

(21) Cosentino, U.; Villa, A.; Piteo, D.; Moro, G.; Barone, V.; Maiocchi, A. *J. Am. Chem. Soc.* **2002**, *124*, 4901.

(22) Tomasi, J.; Persico, M. *Chem. Rev.* **1994**, *94*, 2027.

(23) Matz, W.; Schell, N.; Bernhard, G.; Prokert, F.; Reich, T.; Claussner, J.; Oehme, W.; Schlenk, R.; Dienel, S.; Funke, H.; Eichhorn, F.; Betzl, M.; Pröhl, D.; Strauch, U.; Hüttig, G.; Krug, H.; Neumann, W.; Brendler, V.; Reichel, P.; Denecke, M. A.; Nitsche, H. *J. Synchrotron Rad.* **1999**, *6*, 1076.

(24) Reich, T.; Bernhard, G.; Geipel, G.; Funke, H.; Hennig, C.; Rossberg, A.; Matz, W.; Schell, N.; Nitsche, H. *J. Radiochim. Acta* **2000**, *88*, 633.

(25) George, G. N.; Pickering, I. J. *EXAFSPAK, A Suite of Computer Programs for Analysis of X-ray Absorption Spectra*; Stanford Synchrotron Radiation Laboratory: Stanford, CA, 1995.

(26) Zabinsky, S. I.; Rehr, J. J.; Ankudinov, A.; Albers, R. C.; Eller, M. J. *Phys. Rev. B* **1995**, *52*, 2995.

(27) *X-ray Absorption: Principles, Applications, Techniques for EXAFS, SEXAFS, and XANES*; Koningsberger, D. E., Prins, R., Eds.; Wiley-Interscience: New York, 1988.

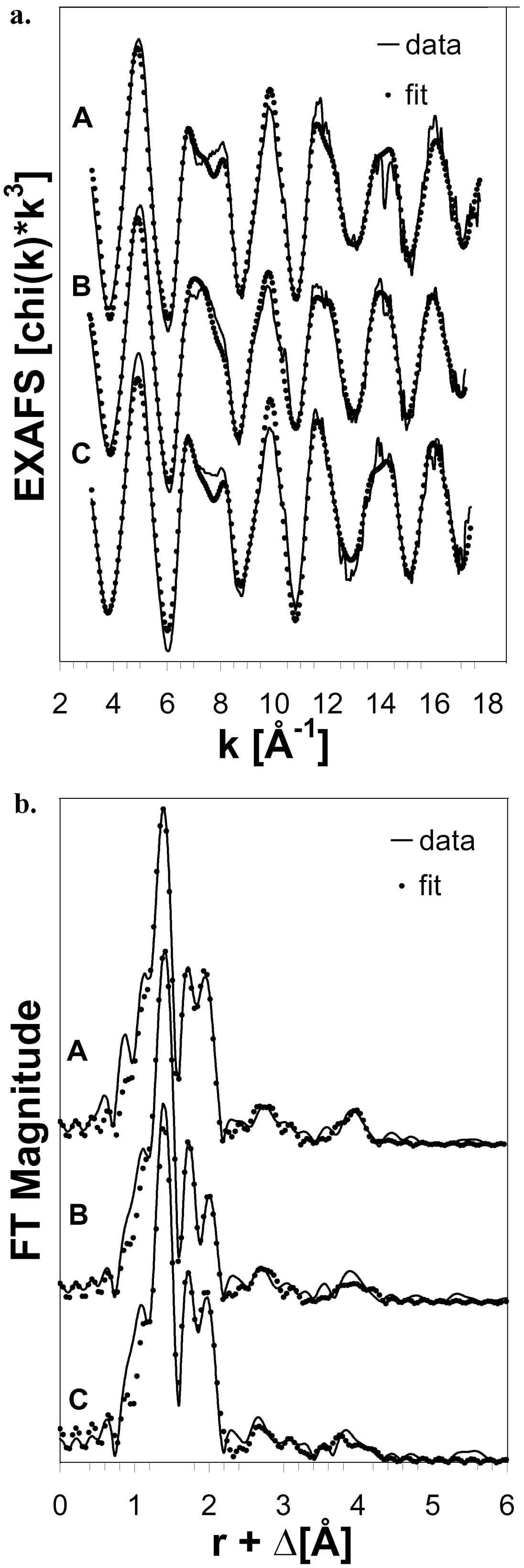

Figure 1. U L_{III} -edge k^3-weighted EXAFS data and corresponding Fourier transforms measured for (A) $UO_2(ox)_2{}^{2-}$(aq), (B) $UO_2(ox)_2F^{3-}$, and (C) $UO_2(ox)_3{}^{4-}$. The solid lines are the experimental data, and the dotted lines represent the best theoretical fits of the data.

four shells to describe the experimental data; only the data for $[UO_2(oxalate)_2F]^{3-}$ justify the use of four shells. Figure 1a and b shows the agreement between experimental and model-based EXAFS oscillations and the corresponding Fourier transforms. The contributions of the different shells in $[UO_2(oxalate)_3]^{4-}$ to the EXAFS oscillations are also given in Table 1. These data can be compared with the distances obtained from solid-state structures and quantum chemical calculations in Tables 2 and 3, respectively. The experimental bond distances obtained from EXAFS data from solutions of $[UO_2(oxalate)_2(H_2O)]^{2-}$ and $[UO_2(oxalate)_2F]^{3-}$ are in good agreement with the theoretical model for the most stable isomer containing two chelate-bonded oxalate ligands, vide infra. The experimental standard deviations in the bond distances obtained from the solid-state structures are, in many cases, large, which obscures a comparison with the other two data sets. The first fitting of the EXAFS data for solutions in which $[UO_2(oxalate)_3]^{4-}$ is the predominant species was made using three shells with N fixed at 2 for the first shell (the $U-O_{yl}$) distance, $N = 4.8 \pm 0.6$ for the equatorial oxygen atoms (the second shell), and $N = 3.8 \pm 0.9$ for the third shell, corresponding to the U−C distances. The uncertainty in the coordination number for the second shell is so large that one cannot distinguish between four-, five-, and six-coordinate isomers. However, the bond distances are much more precise and consistent only with a five-coordinate structure containing two chelate-bonded oxalates and a third bonded through a single carboxylate oxygen. We used this structure to refine the EXAFS fit by fixing the coordination numbers in the second and third shells and optimizing only the U−O and U−C bond distances, as reported in Table 1; the resulting changes in the bond distances between the two models were within the estimated uncertainty. Attempts to fit the experimental data to the other isomers failed.

Results and Discussion

Structure and Thermodynamics. The following discussion is based on the structures and energies reported in Tables 2−5, in Figures 2−7, and in the Supporting Information. The latter contains the geometry optimized in the gas phase, figures not shown in the main text, the coordinates of all atoms in the different complexes, and the vibration frequencies and their intensities.

(a) Structure and Thermodynamics of $UO_2(oxalate)_2(H_2O)^{2-}$ and $UO_2(oxalate)_2F^{3-}$. The structure of the isomer of $UO_2(oxalate)_2(H_2O)^{2-}$ with two chelating oxalate ligands has been discussed in a previous communication,[14] where data obtained by estimating solvent effects with single-point calculations using the gas-phase geometry were used without performing a full geometry optimization in the solvent. One of the focal points in the present study is to investigate the structure and coordination in water by comparing accurate theoretical results with EXAFS data. Hence, we performed a re-optimization in the solvent of the geometry of the two five-coordinate isomers, one with two chelating oxalate ligands and the other with one chelating oxalate and one bonded “end-on” to both oxygen atoms of the same carboxylate group. As in the gas-phase geometry, the two chelating groups are planar and confined to the equatorial plane, resulting in C_s symmetry (cf. Figure 2b). Solvent effects induce an increase of the $U-O_{ox}$ distance by 0.02−0.05 Å and a decrease of the uranium−water distance by 0.08 Å (cf. Table 2). This effect follows the general trends observed on other cation hydrates using extended discrete descriptions of the outer hydration shell.[28−30] The structure in solution differs in some cases significantly from that

Table 2. Calculated[a] Bond Distances in Ångströms for the Various Isomers of Complexes $[UO_2(ox)_2H_2O]^{2-}$ and $[UO_2(ox)_2F]^{3-}$ and Crystal Data for $[UO_2(ox)_2H_2O]^{2-}$ [b]

		shell (Å)						CPCM geom		gas-phase geom	
chemical species	figure (symmetry)	$U-O_{yl}$	$U-O_{ox}$ (chelate)	$U-O_{ox}$ (carbox)	U−C (chelate)	U−C (carbox)	U−L	ΔU(MP2) (kJ/mol)	ΔG°(MP2) (kJ/mol)	ΔU(MP2) (kJ/mol)	ΔG°(MP2) (kJ/mol)
					$[UO_2(ox)_2H_2O]^{2-}$						
crystal data (cf. ref 3)	Fig 2a	1.62	2.49	−	3.27	−	2.44	−	−	−	−
two chelating oxalate (isomer 1)	Fig 2b (C_s)	1.726	2.40(2)	−	3.268(8)	−	2.54	0.0	0.0	0.0	0.0
one chelating group, one bonded end-on (isomer 2)	Fig 2c (C_1)	1.720	2.373(8)	2.50(2)	3.249(4)	2.877	2.51	51.2	49.3	49.8	48.2
					$[UO_2(ox)_2F]^{3-}$						
two chelating oxalate (isomer 1)	Fig 3a (C_s)	1.737	2.432(8)	−	3.307(4)	−	2.219	0.0	0.0	0.0	0.0
one chelating group, one bonded end-on (isomer 2)	Fig 3b (C_1)	1.730	2.402	2.53(1)	3.275	2.909	2.201	9.2	7.5	6.0	2.3

[a] All geometry optimizations were done without symmetry constraints at the HF level in the solvent. The values in parentheses indicate the maximum deviations of individual distances from the average values. The relative energies and free energies, in kilojoules per mole, were determined by single-point MP2 calculations in solvent.

Table 3. Theoretical Data[a] for the Different Isomers of $[UO_2(ox)_3]^{2-}$

			shell (Å)							CPCM geom		gas-phase geom	
isomer	N	structure figure (symm)	$U-O_{yl}$	$U-O_{ox}$ (chelate)	$U-O_{ox}$ (carbox)	$U-O_{ox}$ (uni)	U−C (chelate)	U−C (carbox)	U−C (uni)	ΔU (MP2) (kJ/mol)	ΔG° (MP2) (kJ/mol)	ΔU (MP2) (kJ/mol)	ΔG° (MP2) (kJ/mol)
two chelating groups and one unidentate	5	struct 1 Fig 4a (C_1)	1.730(2)	2.427(6)	−	2.386	3.302(2)	−	3.459	0.0	0.0	0.0	0.0
one chelating group, one bonded end-on, and one unidentate	5	struct 2 Fig 4b (C_1)	1.725(1)	2.398(3)	2.53(1)	2.353	3.271(1)	2.902	3.455	38.3	36.7	32.2	32.1
three chelating groups	6	struct 3 Fig 4c (C_{3h})	1.727(1)	2.52(1)	−	−	3.424(3)	−	−	36.3	b	b	b
two chelating groups and one bonded end-on	6	struct 4 Fig 4d (C_2)	1.724(1)	2.46(2)	2.61(4)	−	3.36(1)	3.000	−	16.8	18.9	14.0	14.8
one chelating group and two bonded end-on	6	struct 5 Fig 4e (C_{2v})	1.723	2.432(1)	2.58(1)	−	3.317(1)	2.959	−	20.3	21.4	14.7	15.4
one chelating group and two unidentate	4	struct 6 Fig 4f (C_2)	1.725(1)	2.384(3)	−	2.325(8)	3.258(2)	−	3.42(2)	85.9	77.5	78.7	78.3

[a] All geometry optimizations were done without symmetry constraints at the HF level in the solvent. The bond distances are in ångströms, and N denotes the coordination number in the equatorial plane. The values in parentheses indicate the maximum deviations of individual distances from the average value. The relative energies and free energies, in kilojoules per mole, were determined by single-point MP2 calculations in solvent (CPCM model) using the geometry optimized either in solvent (CPCM) or in the gas phase. [b] Structure 3 is not stable in the gas phase.

obtained from X-ray data in the solid state[3] (cf. Table 2 and Figure 2a and b). This is in part due to systematic errors in the crystal structure determination as indicated, for example, in $U-O_{yl}$ distances that deviate significantly from 1.75 Å. In the solid state, the oxalate ligands are planar but tilted out of the equatorial plane to act as bridges between two uranyl ions, a constraint that is not present in solution.

The calculated energy difference between the two isomers is 49.3 kJ/mol in solvent. This fact, together with the experimental data, indicates that the isomer in Figure 2b is the predominant one.

Two five-coordinate isomers also exist for $UO_2(oxalate)_2F^{3-}$, where the one with two chelating oxalates is the most stable but the energy difference from the structure including one chelate and one oxalate bonded end-on is only 7.5 kJ/mol. This indicates that the two isomers can coexist in solution and that the exchange between them can take place by oxalate ring opening, followed by rotation and end-on binding to one carboxylate group. We will return to this issue when discussing exchange mechanisms. The energy difference between the two isomers in $UO_2(oxalate)_2(H_2O)^{2-}$ is much larger, 49 kJ/mol. There are significant differences, 0.1 Å, in the $U-O_{ox}$ bond distance between the two isomers (cf.

---

(28) Pullman, A. In *Quantum Theory of Chemical Reactions*; Daudel, R., Pullman, A., Salem, L., Veillard, A., Eds.; Reidel Publishing Co.: Dordrecht, The Netherlands, 1981; Vol. II.

(29) Claverie, P.; Daudey, J. P.; Langlet, J.; Pullman, B.; Piazzola, D.; Huron, M. J. *J. Phys. Chem.* **1978**, *82*, 405.

(30) Martínez, J. M.; Pappalardo, R. R.; Marcos, E. S.; Mennucci, B.; Tomasi, J. *J. Phys. Chem. B* **2002**, *106*, 1118.

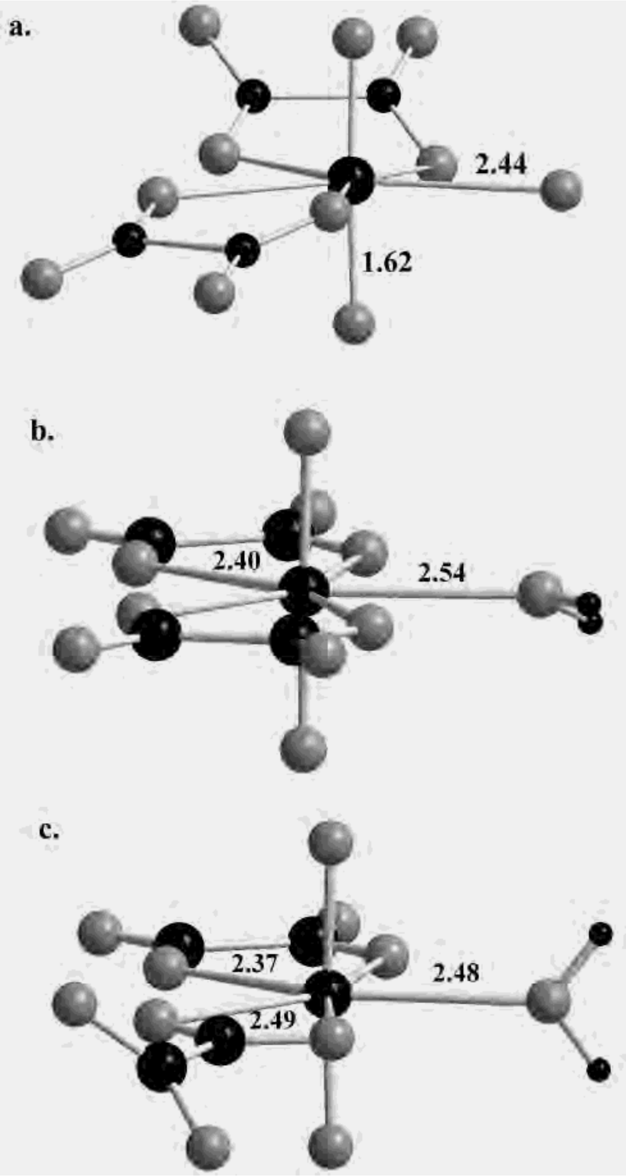

Figure 2. Perspective views of the crystal structures and isomers of $[UO_2(oxalate)_2(H_2O)]^{2-}$ optimized in the solvent (CPCM model): (a) X-ray crystal structure (cf. ref 3), (b) ground-state isomer 1 with two chelating oxalate groups, and (c) isomer 2 with one chelating oxalate group and one bonded end-on. The uranium atom and the carbon and hydrogen atoms are black, and the oxygen atoms are gray. Distances are in ångströms.

Table 2 and Figure 3a and b), which makes it possible to identify the coordination mode in solution. The bond distances for the isomer with two planar chelating oxalate groups (cf. Figures 2b and 3a) are in excellent agreement with the EXAFS data, within 0.01 Å for the U−F distance and within 0.04 Å for the $U-O_{ox}$ and U−C distances in both $UO_2(oxalate)_2(H_2O)^{2-}$ and $UO_2(oxalate)_2F^{3-}$. This is within the width of the radial distribution, 0.08 Å estimated from the Debye−Waller factor (cf. Table 1). The internal uranyl distance is 0.05 Å shorter than the experimental value; this is a common feature for uranyl complexes, and the difference is known to vanish at the correlated level, as discussed in ref 12. The good agreement between experimental and theory-based U−F distances has already been noted for $UO_2F_4(H_2O)^{2-}$ (cf. ref 13).

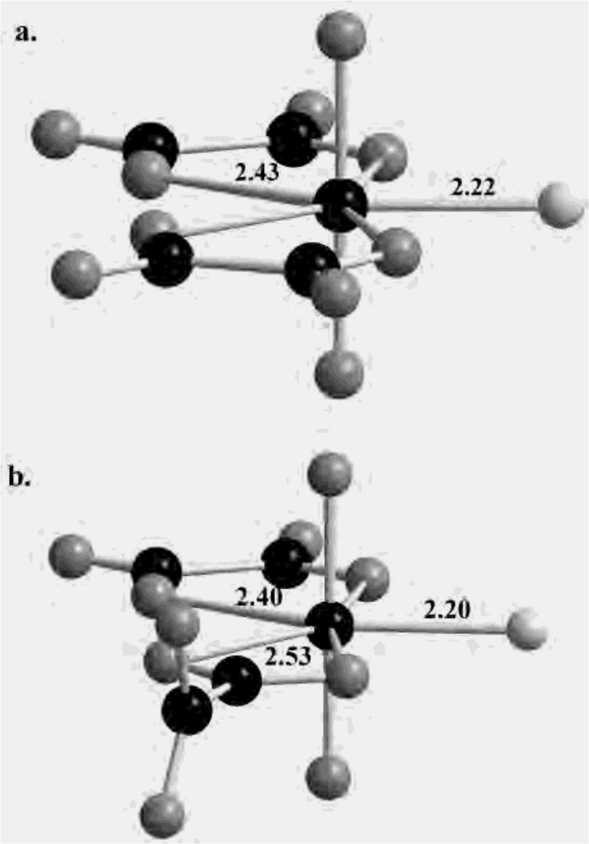

Figure 3. Perspective views of the various isomers of $[UO_2(oxalate)_2F]^{3-}$ optimized in the solvent (CPCM model): (a) ground-state isomer 1 with two chelating oxalate groups and (b) isomer 2 with one chelating oxalate group and one bonded end-on. Distances are in ångströms.

(b) Structure and Thermodynamics of the $UO_2(oxalate)_3^{4-}$ Isomers. We have identified three six-coordinate, two five-coordinate, and one four-coordinate isomer of $UO_2(oxalate)_3^{4-}$. The six-coordinate isomers contain three chelate-bonded oxalate groups (structure 3), two chelate-bonded oxalates and a third bonded end-on to one carboxylate group (structure 4), one chelate-bonded oxalate, and two oxalates bonded end-on to a single carboxylate group (structure 5). One of the five-coordinate isomers contains two chelate-bonded oxalates with the third bonded to a single carboxylate oxygen atom (structure 1); the other contains one chelate-bonded oxalate, one oxalate coordinated end-on to two oxygen atoms of the same carboxylate group, and one bonded through a single carboxylate oxygen (structure 2). The four-coordinate isomer contains one chelate-bonded oxalate and two bonded through a single carboxylate oxygen (structure 6). Bond distances at the Hartree−Fock level and the relative energy at the MP2 level of the different isomers are given in Table 3, the structures are shown in Figure 4, and structural elements from single-crystal data of solid uranium oxalate compounds are included in the Supporting Information as Figures S1−S3. The effect of correlation on the relative energy is small, 10 kJ/mol or less (cf. Table 3). Solute−solvent interactions induce an increase of the $U-O_{ox}$ distance by 0.02−0.08 Å (cf. Tables 3 and S2). The five-coordinate structure 1 is the most stable and should therefore be the predominant one in solution. This is confirmed by

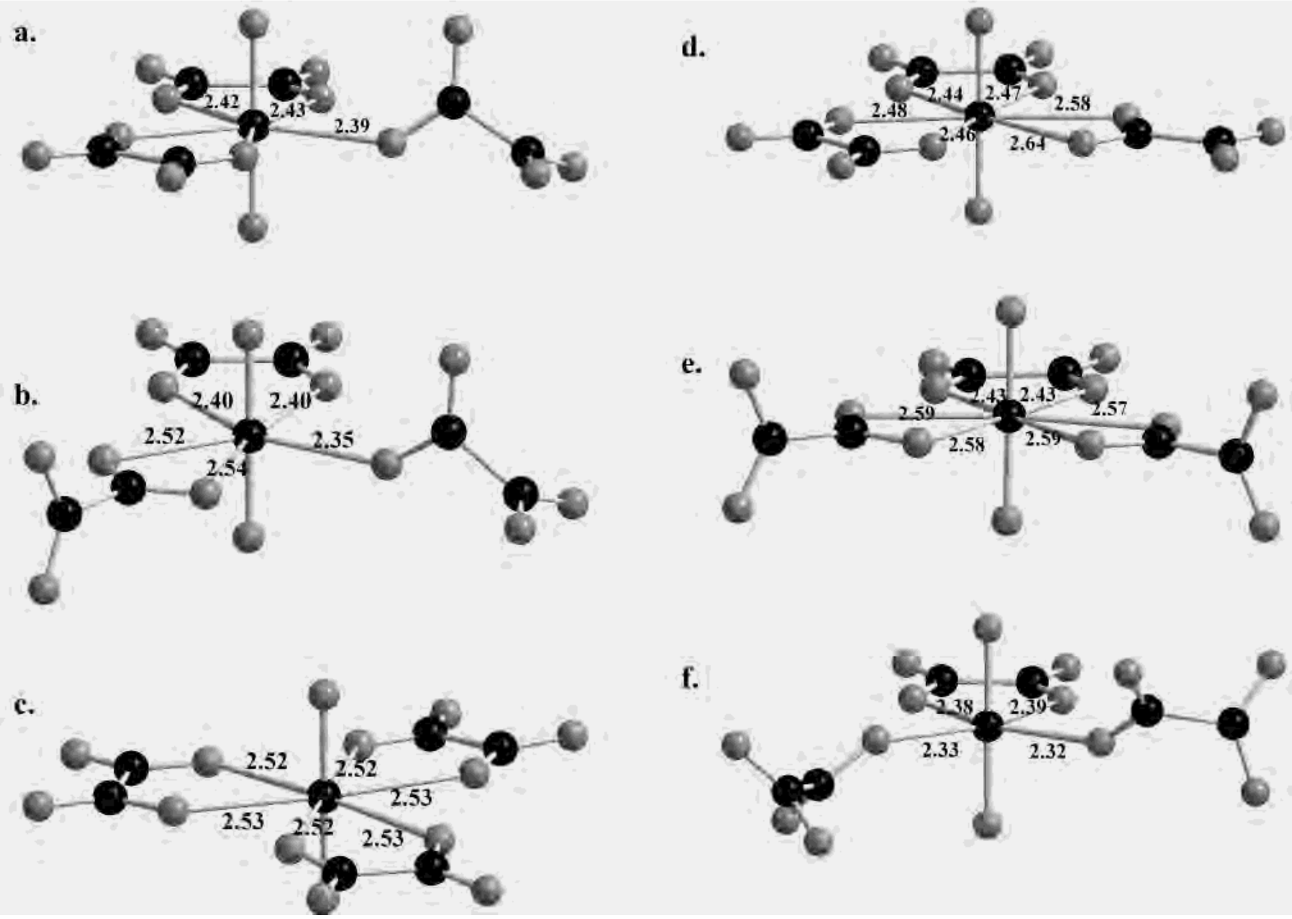

Figure 4. Perspective views of $[UO_2(oxalate)_3]^{4-}$ isomers optimized in the solvent (CPCM model): (a) ground-state isomer structure 1, (b) structure 2, (c) structure 3, (d) structure 4, (e) structure 5, and (f) structure 6. Distances are in ångströms.

comparing the bond distances with the experimental EXAFS data; the experimental and theory-based bond distances agree to within 0.05 Å for the $U-O_{ox}$ and U−C distances (cf. Table 1). The agreement in bond distances between theoretical and solid-state structures is also satisfactory; however, the accuracy of some of the latter results is not particularly high. The main difference between the structures determined by theory and those obtained from X-ray data is the conformation of the ligands (cf. Figures 4 and S1−S3); this is not surprising as one refers to a solvent model and the other to the solid state.

There is a systematic trend in the U−O distances in the chelate-bonded oxalate, with the shortest distance, 2.38 Å, being found in the four-coordinate isomer. The distances are very near the same in all five-coordinate isomers, 2.40−2.43 Å, whereas they are about 2.43−2.52 Å in the six-coordinate isomers. It seems reasonable to attribute this trend to increasing repulsion between oxygen atoms in the coordination plane with increasing coordination number. The bond distance between U and the carboxylate group bonded end-on is always significantly greater, 0.15 Å, than that in the chelate, as already noticed in $UO_2(oxalate)_2F^{3-}$.

All six-coordinate $UO_2(oxalate)_3^{4-}$ isomers are less stable than the five-coordinate ground-state structure 1, structures 4 and 5 by 17 and 20 kJ/mol, respectively, and structure 3 by 36 kJ/mol. The five-coordinate structure 2 containing only one chelate has an energy that is 38 kJ/mol above the ground state, whereas the four-coordinate structure 6 is 86 kJ/mol higher. As for $UO_2(oxalate)_2F^{3-}$, the energy difference between a chelating oxalate group and one bonded end-on is small, 19 kJ/mol between structures 3 and 4 and only 3.5 kJ/mol between structures 4 and 5.

(c) $UO_2(oxalate)_3^{4-}$ in Solution: Comparison with Equilibrium Constant Data. The stepwise equilibrium constants, log K_{n+1}, for the reaction

$$UO_2(oxalate)_n^{2-2n} + oxalate^{2-} \leftrightarrows UO_2(oxalate)_{n+1}^{-2n}, \quad n = 0-2 \qquad (2)$$

have been determined experimentally by Havel[8a] (log $K_1 = 5.99$, log $K_2 = 4.65$, log $K_3 = 0.36$) and by Ferri et al.[9] (log $K_1 = 6.20$, log $K_2 = 5.01$, log $K_3 = 3.69$). The large values of the first two equilibrium constants indicate a significant chelate effect. log K_3 from Ferri et al.[9] indicates that the third ligand also forms a chelate, whereas that from Havel[8a] indicates unidentate coordination. In one of our previous studies,[31] we measured the concentrations of oxalate^{2-} and $UO_2(oxalate)_2^{2-}$(aq) from the corresponding integrals in ^{13}C NMR spectra over a fairly large range of oxalate concentrations. We calculated the speciation in these test solutions using the two sets of equilibrium constants given above. The

---

(31) Aas, W.; Szabó, Z.; Grenthe, I. *J. Chem. Soc., Dalton Trans.* **1999**, 1311.

Table 4. Theoretical Data[a] for $[UO_2(ox)F_3]^{3-}$

chemical species	structure figure (symm)	shell (Å)					CPCM geom		gas-phase geom	
		$U-O_{yl}$	$U-O_{ox}$	$U\cdots O_{ox}$	$U-C$	$U-F$	ΔU(MP2) (kJ/mol)	$\Delta G°$(MP2) (kJ/mol)	ΔU(MP2) (kJ/mol)	$\Delta G°$(MP2) (kJ/mol)
chelating oxalate (isomer 1)	struct 7 Fig 5a (C_{2v})	1.750	2.482	–	3.358	2.252(2)	0.0	0.0	0.0	0.0
chelate opening (TS)	TS_{7-8} Fig 5b (C_1)	1.742	2.376	3.600	3.505, 4.020	2.232(5)	63.1	58.7	48.2	45.0
unidentate oxalate (intermediate)	struct 8 Fig 5c (C_1)	1.741(1)	2.379	–	3.432	2.222(4)	47.3	36.7	47.4	35.4
carbox closure (TS)	TS_{8-9} Fig 5d (C_1)	1.742(0)	2.432	3.313	3.235, 4.673	2.224(4)	55.8	52.7	38.7	36.5
oxalate group bonded end-on (isomer 2)	struct 9 Fig 5e (C_{2v})	1.745	2.56(1)	–	2.994	2.235(3)	17.8	14.1	15.5	10.9

[a] All geometry optimizations were done without symmetry constraints at the HF level in the solvent. Bond distances are in ångströms. The values in parentheses indicate the maximum deviations of individual distances from the average value. The relative energies, in kilojoules per mole, were determined by single-point MP2 calculations in solvent.

results are shown in Figure S4 of the Supporting Information, and the corresponding ^{13}C NMR spectra is in Figure S5; these spectra are consistent only with the equilibrium constants of Havel, but not with those of Ferri et al. This fact, in addition to the structure determination of $UO_2(oxalate)_3^{4-}$ in solution and the relative energy of the tris-oxalate isomers, provides a strong indication that one of the oxalate ligands coordinates through a single carboxylate oxygen. In a recent paper, Havel et al.[8b] reinvestigated the uranyl(VI)–oxalate system using spectrophotometry, and they now claim a chemical model different from the one they first proposed[8a] that, in addition to the mononuclear complexes, also contains two binuclear species. This equilibrium model is not consistent with the equilibrium data of Ferri et al. or with our NMR and EXAFS data.

(d) Structure and Thermodynamics of $UO_2(oxalate)F_3^{3-}$ Isomers. The structures and relative energies of two five-coordinate isomers (structures 7 and 9) are given in Table 4 and Figure 5. The most stable isomer contains a chelate-bonded oxalate, and also in this case, the energy difference between the isomers is small, 18 kJ/mol. In a previous experimental study,[15] we determined the activation energy for the exchange of oxalate and fluoride in this complex, and we will discuss these data in the next section.

Rates and Mechanisms of Ligand Exchange Reactions. We will begin the discussion of reaction mechanisms by using experimental activation enthalpies and theoretical activation energies, $\Delta U^{\ddagger}$, for the ternary UO_2LF_3 complex,[15] where L is a bidentate ligand, oxalate or picolinate, and then continue with the discussion of intramolecular exchange mechanisms between the different isomers of $UO_2(oxalate)_3^{4-}$.

Only the $UO_2(oxalate)F_3^{3-}$ system could be studied using quantum chemical methods, as the nonsymmetric picolinate ligands are too large to be handled. Most of the computed activation parameters refer to single-point MP2 calculations in the solvent using the solvent-optimized geometry, with an exception for the less favorable intramolecular exchange pathways A and C in $UO_2(oxalate)_3^{4-}$ (cf. Scheme 2), where the transition state geometries were optimized only in the gas phase.

First, we make a general remark regarding the importance of solvent effects on the calculated quantities, on the basis of a comparison of the structural data for $UO_2(oxalate)F_3^{3-}$ presented in Tables 4 and S3. In the solvent, all $U-O_{ox}$ distances in the equatorial plane decrease by 0.04–0.10 Å; this change, as compared to the gas phase, is the same for all isomers. These changes are so small that they do not result in a significant change in the size of the cavity used in the solvent model (cf. Supporting Information). Therefore, we do not expect large changes in the relative stabilities of the isomers when using the gas-phase geometry to estimate the energies in the solvent, as already noticed for the uranyl aqua ion.[14] However, in the transition state the difference between the gas-phase- and solvent-optimized geometries is much larger, up to 0.3 Å, in the distance between U and the leaving/entering group; still the resulting change in the cavity size is small (cf. Supporting Information). However, we know from a previous study that the CPCM model does not fully account for the hydration when there is charge separation, as in the transition state,[16] and that the large increase in the bond distance is an artifact of the simplified solvent model. A more elaborate model always leads to smaller changes (cf. ref 16). However, it should also be noticed that the potential surface is very flat in the vicinity of the transition state.

(a) Intra- and Intermolecular Exchange Reactions in the Ternary Complexes $UO_2LF_3^{3-}$. The intra- and intermolecular reactions in the ternary complexes $UO_2LF_3^{3-}$ will be discussed in terms of Scheme 1, where $X-COO^-$ represents the bidentate ligand L ($X = -COO^-$ for oxalate and $-C_5H_5N$ for picolinate). Both reactions involve a ring opening as the first step; when this is followed by a ligand rotation and ring closure, there will be an apparent exchange between F(A) and F(B) that can only be studied experimentally for asymmetric L ligands. For symmetric ligands such as oxalate, the reaction must be studied by theory. Structure

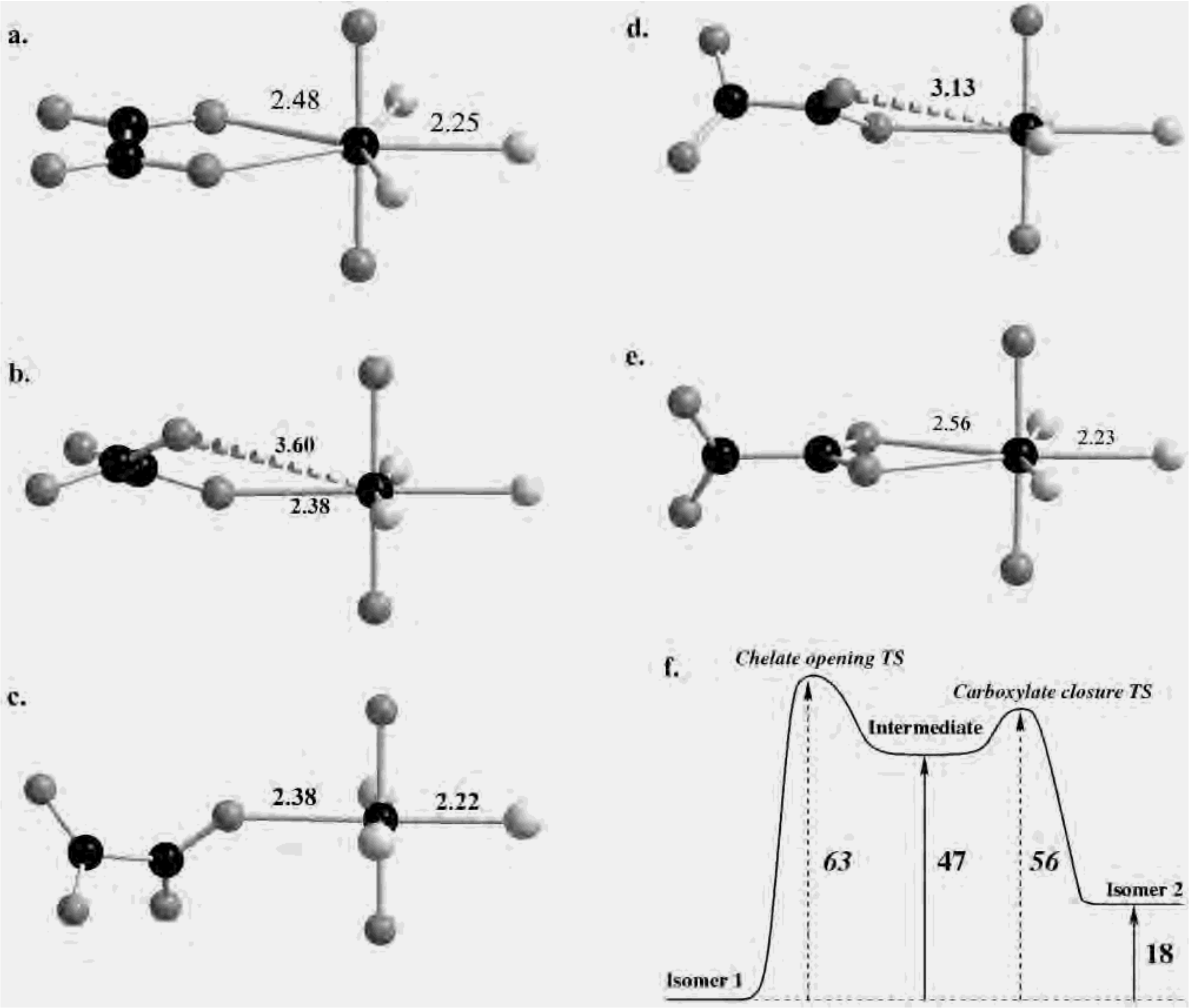

Figure 5. Perspective views of the $[UO_2(oxalate)F_3]^{3-}$ isomers and of the transitions states optimized in the solvent (CPCM model) and reaction profile (f). (a) Ground-state isomer structure 7, (b) chelate opening transition state TS_{7-8}, (c) intermediate structure 8 with the oxalate group bonded to one carboxylate oxygen, (d) carboxylate closure transition state TS_{8-9}, and (e) isomer structure 9. Distances are in ångströms.

Scheme 1. Intramolecular Exchange Pathway in the Ternary Complexes $UO_2LF_3{}^{3}-$, where X−COO− Represents the Bidentate Ligand L (X = −COO− for Oxalate and $-C_5H_5N$ for Picolinate)

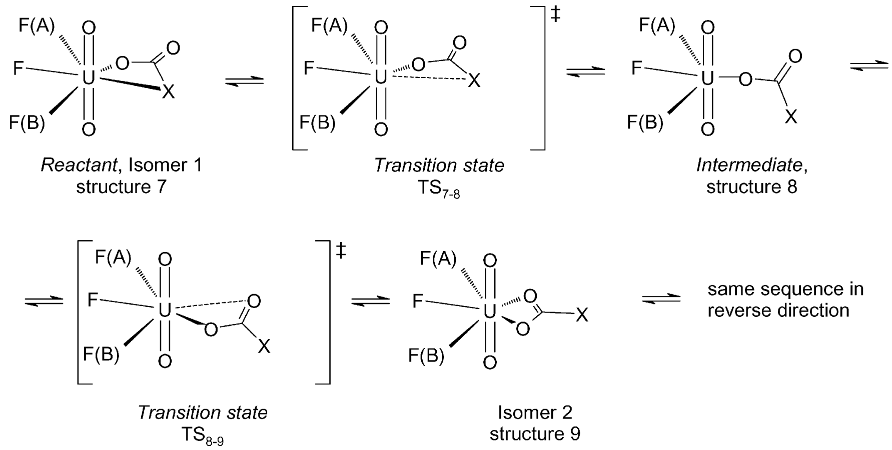

7 is the predominant oxalate isomer, and there is no experimental evidence for the presence of significant amounts of Structure 9 in solution. The intramolecular exchange between the two isomers in a computer experiment involves a chelate ring opening followed by the formation of an intermediate through ring closure at the carboxylate end; by the reverse sequence, we then return to Structure 7, a process that results in ligand rotation for nonsymmetric ligands L.

Scheme 2. Mechanisms for Intramolecular Oxalate Exchange in $[UO_2(oxalate)_3]^{4-}$

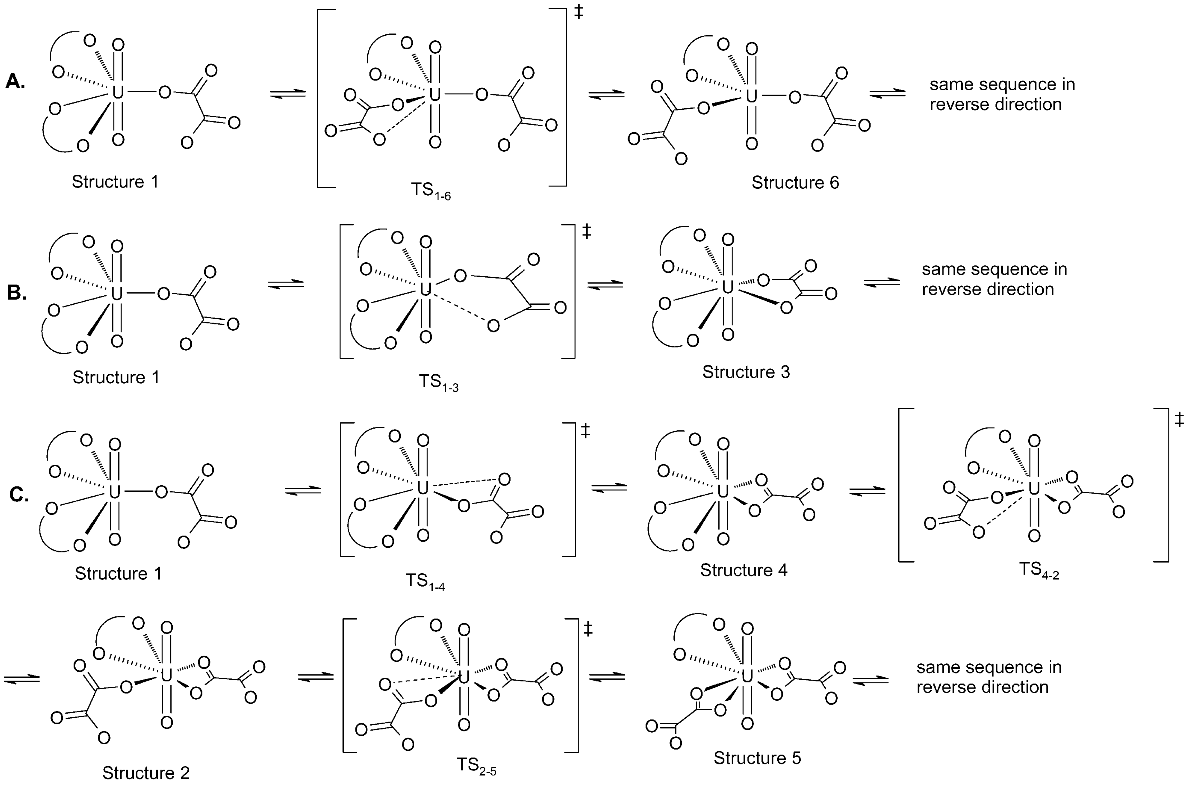

Intermolecular exchange of L has been investigated experimentally,[11,15] but would be very difficult to study by quantum chemical methods, because the charge of the system changes along the reactions path,[16] making the CPCM results somewhat uncertain. However, as the intermolecular reaction must involve an intramolecular chelate ring opening/ring closure, leading to the ring-opened intermediate (structure 8), there is a mechanistic link between the two reactions.

Chelate ring opening is the slow step in the intramolecular exchange reactions between F(A) and F(B). The average experimental value of the activation enthalpy for picolinate systems, $\Delta H^{\ddagger} = 45 \pm 5$ kJ/mol, reported in Table 1 of ref 15, is close to that for the oxalate system obtained from theory, $\Delta U^{\ddagger} = 63$ kJ/mol. We suggest that the chelate ring opening takes place without assistance of water, because the short bond U−F distances would result in a significant "crowding" of the transition state in the A and *I* mechanisms. In addition, water in the second coordination sphere will preferentially be hydrogen bonded to coordinated fluoride and thereby prevent access to uranium; this is consistent with the change in mechanism of water exchange[14] from associative in $UO_2(oxalate)_2(H_2O)^{2-}$ to dissociative in $UO_2F_4(H_2O)^{2-}$. The oxalate ring opening/ring closure in $UO_2(oxalate)F_3^{3-}$ might involve the isomer with oxalate bonded to both oxygen atoms of the same carboxylate group as a second intermediate, but the ligand "rotation" could also take place from the intermediate with Structure 8.

We have previously discussed[15] the mechanism for intermolecular L exchange in $UO_2LF_3^{3-}$. For the picolinate and oxalate systems, we found that the activation enthalpies are 60 ± 3 and 70 ± 6 kJ/mol, respectively. The very similar experimental and theory-based activation enthalpies for the ring opening in the oxalate and picolinate systems and the similar experimental activation enthalpy for the intermolecular L exchange indicate similar mechanisms. The rate constants for oxalate and picolinate exchange at −5 °C are practically the same at 6.2 ± 0.2 and 4.7 ± 0.2 s^{-1}, respectively. These facts make us believe that the detailed mechanistic analysis for the oxalate system is also applicable to other systems where L is a bidentate ligand.

(b) Intramolecular Exchange Reactions between $UO_2(oxalate)_3^{4-}$ Isomers. No direct experimental data are available for reactions of this type; however, such reactions involve chelate ring-opening/ring-closure reactions of the type discussed for the $UO_2LF_3^{3-}$ complexes (Scheme 1). The only experimental kinetic information available refers to the rate and mechanism of the intermolecular exchange reaction

$$UO_2(oxalate)_2(H_2O)^{2-} + {}^*oxalate^{2-} \leftrightarrows UO_2({}^*oxalate)_2(H_2O)^{2-} + oxalate^{2-} \quad (3)$$

This reaction has an activation enthalpy of 31 ± 2 kJ/mol, as determined by ^{13}C NMR measurements;[31] the NMR spectra exhibited two broad peaks, one for the complex and one for the free ligand (cf. Figure S6 in the Supporting Information), indicating rapid exchange on the NMR time scale within the complex. The exchange reaction consists of several steps, at least one of which must involve chelate ring opening/ring closure that can be explored using the theory method discussed in the preceding text. The chemically most reasonable intramolecular exchange mechanisms are given in Scheme 2, with the corresponding transition state

Table 5. Geometries[a] of the Transition States and Activation Energies for Mechanisms A−C of the Intramolecular Exchange in $UO_2(ox)_3^{4-}$

		shell (Å)								
transition state	figure (symm)	$U-O_{yl}$	$U-O_{ox}$ (chelate)	$U-O_{ox}$ (carbox)	$U-O_{ox}$ (uni)	$U\cdots O_{ox}$[b]	$\Delta U_m^{\ddagger}$	$\Delta U_n^{\ddagger}$	$\Delta G_m^{\ddagger}$	$\Delta G_n^{\ddagger}$
				mechanism A						
trans chelate opening (struct 1 → struct 6)	TS_{1-6} Fig S4b (C_1)	1.722(2) 1.722(1)	2.45(1) 2.44(1)	− −	2.365 2.386	2.354, 3.558 2.354, 3.507	85.0 93.7	6.3 15.0	82.0 90.7	4.5 13.2
				mechanism B						
chelate closure (struct 1 → struct 3)	TS_{1-3} Fig 7 (C_1)	1.720(1)	2.547(1)			2.557, 2.749	27.9 38.0[d]	*c* 2.0(3)	26.7	*c*
				mechanism C						
carboxylate closure (struct 1 → struct 4)	TS_{1-4} Fig S7a (C_1)	1.722	2.52(1)			2.588, 2.789	15.5	1.5	14.5	−0.4
chelate opening (struct 4 → struct 2)	TS_{4-2} Fig S7b (C_1)	1.719(3)	2.49(1)	2.61(5)		2.433, 3.031	25.1	6.9	22.9	5.7
carboxylate closure (struct 2 → struct 5)	TS_{2-5} Fig S7c (C_1)	1.721	2.48(1)	2.60(2)		2.487, 3.029	1.2	18.8	−0.2	16.5

[a] Geometries of the transition states were optimized in the gas phase at the Hartree−Fock level. The structure of transition state TS_{1-3} was reoptimized in the solvent. The parenthesis denotes the maximum deviations of individual distances from the average values. Distances are in ångströms. For every mechanistic step starting with structure m and going to structure n, we calculated the activation energy $\Delta U_m^{\ddagger}$, and free energy of activation $\Delta G_m^{\ddagger}$, as well as the relative energy and free energy between the transition state and structure n, $\Delta U_n^{\ddagger}$ and $\Delta G_n^{\ddagger}$, respectively. These are single-point MP2 calculations in solvent using the optimized structures in the gas phase. [b] The first and second $U\cdots O_{ox}$ values refer to the distance to the coordinated oxygen end and moving oxygen atom, respectively, in the opening/closing oxalate group. [c] Structure 3 is not stable in the gas phase. [d] Single-point MP2 calculation in solvent using geometries optimized in solvent.

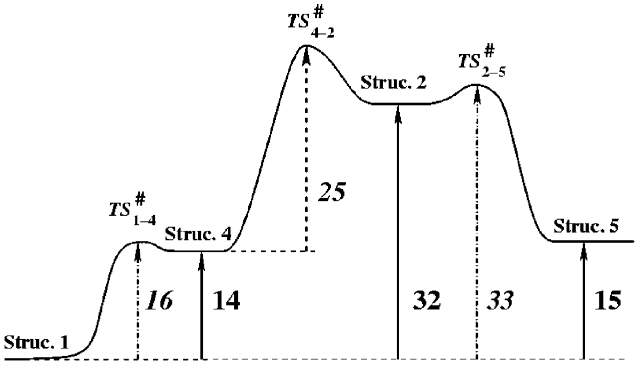

Figure 6. Energy reaction profile for mechanism C using gas-phase optimized structures. All energies are in kJ/mol (cf. Tables 5 and 3).

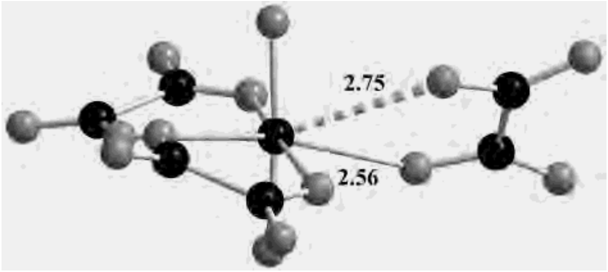

Figure 7. Perspective view of the transition state (TS_{1-3}) in mechanism B, going from the reactant with two chelating oxalate groups and one singly bonded oxalate group (structure 1) to the intermediate with three chelating oxalate groups (structure 3). The geometry was optimized in the gas phase. The dashed line denotes the distance to the entering/leaving oxygen atom. Distances are in ångströms.

geometries and activation energies listed in Table 5; some consist of many steps involving intermediates and transition states, such as mechanism C in Scheme 2. The reaction profiles must be symmetric, so only one-half of the mechanism (including structures 6, 3, and 5) is shown in Scheme 2 and in the energy−reaction coordinate diagrams (Figure 6). Two of the exchange pathways involve only one intermediate; mechanism A is a chelate ring opening leading to a four-coordinate intermediate (structure 6, cf. Figure S6) with an activation energy (85 kJ/mol) that is significantly higher than those for the other pathways and also larger than that found in $UO_2(oxalate)F_3^{3-}$. Mechanism B involves chelate ring closure to the six-coordinate tris-chelating intermediate (structure 3), with an activation energy of 28 kJ/mol (cf. Figure 7). By re-optimizing the geometry of the transition state in solvent, we observed that the distance to the entering/leaving carboxylate oxygen increased by 0.2 Å as observed in the ternary complexes and that the activation energy increased from 28 to 38 kJ/mol. The energy difference, 2 kJ/mol, between the intermediate and the transition state indicates a very short lifetime of the former. Mechanism C consists of many steps; however, the activation energy between the intermediates with structures 4 and 2 and transition states TS_{1-4} and TS_{2-4} are small, 1.5 and 6.9 kJ/mol, respectively. This is less than the thermal energy at 300 K and we can therefore describe the reaction with an "effective" reaction pathway from structure 1 to structure 5 with one activation energy of 41 kJ/mol (16 + 25 kJ/mol). On the basis of the quantum chemical calculations using the gas-phase geometry, we conclude that the most favored pathway for intramolecular exchange in $UO_3(oxalate)_3^{4-}$ involves the tris-chelated intermediate (structure 3), which has an activation energy that is 13 and 57 kJ/mol lower than those for pathways A and C, respectively.

There is an additional mechanistic detail that is not apparent from Scheme 2: the chelate ring opening from structure 1 can take place either in the cis or trans position from the unidentate oxalate. The cis opening involves less interference with adjacent ligands and has an activation energy that is 9 kJ/mol lower than that of the trans opening.

(c) Exchange Mechanisms in UO_2L_2A Complexes, where A is a Unidentate Ligand. If L is an asymmetric bidentate ligand, there are two possible orientations of the ligand, resulting in two isomers. It was not possible to study the intramolecular exchange in the $UO_2(picolinate)_2F^-$ system in water experimentally; instead, the reaction was investigated in CD_3OD and dimethyl sulfoxide. The activation energies in the two solvents are 26.9 and 45.9 kJ/mol, respectively, indicating a very strong solvent dependence. This is consistent with an A mechanism involving the solvent as observed for the water exchange in $UO_2(oxalate)_2(H_2O)^{2-}$. The intermolecular exchange of oxalate in $UO_2(oxalate)_2F^{2-}$ has been studied experimentally, and the activation enthalpy is $\Delta H^{\ddagger} = 43 \pm 3$ kJ/mol. This reaction must involve the opening of the oxalate chelate ring, and accordingly, the activation enthalpy for this process must be lower than 43 kJ/mol. Some preliminary ab initio calculations on $UO_2(oxalate)_2F^{3-}$ led to a value of 87 kJ/mol. The high barrier for this purely dissociative ring opening indicates that it cannot be the first step in the mechanism; a water-assisted reaction might result in lower activation energy as a result of hydrogen bonding between the water molecule and the coordinated ligand. However, this is still speculative, and we are presently exploring this hypothesis.

Conclusions

We have shown that the geometry of dioxouranium(VI) complexes can be accurately predicted using quantum chemical methods; the difference between calculated and experimental bond distances is generally less than 0.03−0.05 Å. Quantum chemical methods can also be used to predict the relative energies of structural isomers that agree well with experimental data. Theoretical methods are therefore important when selecting models for the interpretation of solution EXAFS data of complexes for which solid-state structures are not available.

We have tested the effect of solvent models on the structures and energies of dioxouranium(VI) complexes, as compared to the corresponding quantities in the gas phase. For ground states, the two models are in good agreement, with differences in bond distance and energy typically of less than 0.06 Å and 10 kJ/mol, respectively. However, there might be a significant difference in the distance between uranium and the leaving/entering group in the transition state. This results in a systematic error of about 10 kJ/mol when the gas-phase geometry is used to estimate the activation energy in solution; however, the difference in activation energy between different pathways is expected to be smaller.

A comparison of the experimental activation enthalpies, $\Delta H^{\ddagger}$(298 K), for the intra- and intermolecular exchanges in $UO_2(oxalate)F_3^{3-}$ with the theory-based activation energy for the chelate-opening step provides a strong indication that both reactions begin with a chelate ring-opening step without any water assistance. The situation might be different in $UO_2(oxalate)_2L$ complexes where the computed activation energy for the chelate-opening step is twice as large as that obtained experimentally.

No direct experimental information is available on the intramolecular exchange mechanism in $UO_3(oxalate)_3^{4-}$. We have explored three different reaction pathways starting from the five-coordinate isomer. The computed activation energies indicate that the intramolecular exchange follows a mechanism in which a tris-chelated intermediate is formed; the activation energy using geometries optimized in the CPCM solvent is 38 kJ/mol.

Acknowledgment. This study was financially supported by grants from the Carl Trygger Foundation and from Deutsche Forschungsgemeinschaft (V.V.). The EU also supported part of this study through a grant for beamtime at the Rossendorf beamline (ROBL) at ESRF, Grenoble, France and through contract FIKW-CT-2000-00035 (ACTAF). In this context, we thank the team at ROBL (T. Reich, C. Hennig, A. Rossberg, and H. Funke) for all their assistance.

Supporting Information Available: All crystal and computed structures not presented in the text (Figures S1−S3, S6−S7); equilibrium distribution diagrams for the binary uranium(VI)−oxalate system (Figure S4); fluoride NMR spectra for the binary uranium(VI)−oxalate system (Figure S5); structural data for all structures optimized in the gas phase and not presented in the main text (Tables S1−S3); coordinates and total energies of all computed structures (Tables S4); frequencies calculated in the gas phase of all ground-state isomers (Table S5). This material is available free of charge via the Internet at http://pubs.acs.org.

IC026068S